Title:

Directional Peak Factors of Strong-Motion Response Spectra: A Stochastic Field Representation on the Circle

Authors:

Rajesh Rupakhety[1]

Víctor M. Hernández-Aguirre[2]

[1] Earthquake Engineering Research Centre, Faculty of Civil and Environmental Engineering, University of Iceland, Austurvegur 2a, 800 Selfoss, Iceland

Email: rajesh@hi.is

[2] Earthquake Engineering Research Centre, Faculty of Civil and Environmental Engineering, University of Iceland, Austurvegur 2a, 800 Selfoss, Iceland

Email: victorh@hi.is

Preprint Statement

This manuscript is a preprint and has not undergone peer review.

The manuscript is currently under review in Bulletin of Earthquake Engineering.

This version is posted on EarthArXiv to ensure transparency, accessibility, and timely dissemination of the research.

The final published version, if accepted, may differ from this preprint.

Date of Preprint Posting:
20 February 2026

Directional Peak Factors of Strong-Motion Response Spectra: A Stochastic Field Representation on the Circle

Rajesh Rupakhety[1*], Victor Moises Hernández-Aguirre[1]

Abstract

Directional variability in horizontal earthquake ground motions is often addressed using orientation-independent intensity measures obtained by rotating the two horizontal components and summarizing the resulting response spectra. In contrast, the stochastic structure of directional peak factors, which connect second-order response measures to extreme response levels, has received limited attention. This paper presents a systematic empirical characterization of the directional peak-factor field associated with horizontal elastic response spectra. Using a large, uniformly processed strong-motion dataset, directional peak factors are analyzed as a function of oscillator period and orientation. Working in logarithmic space, we decompose the directional peak-factor field into a period-dependent mean and a zero-mean directional fluctuation field that is π-periodic in orientation. Angular dependence is quantified using correlation diagnostics and harmonic decomposition. The results show that directional peak-factor variability exhibits smooth angular structure, with strong correlation across nearby orientations and a consistent zero crossing of angular autocorrelation at 45°. Harmonic analysis demonstrates dominance of the lowest admissible angular mode across all periods considered. The dominant angular harmonic exhibits a consistently nonzero amplitude, weak period dependence, and a phase that is effectively uniform across records. The associated harmonic coefficients are approximately Gaussian and isotropic in the cosine–sine coefficient space, allowing the stochastic structure of directional peak-factor variability to be summarized by a single, smoothly varying scale parameter. This characterization clarifies the dependence structure underlying rotation-based intensity measures and how uncertainty should be interpreted when peak response is summarized across orientation.

Keywords: response spectra; peak factor; ground motion directionality; random vibration

1. Introduction

Peak factors link second-order descriptions of random response (e.g., variance or root-mean-square (RMS) measures) to the extreme values used in engineering decision-making. In many vibration and reliability settings, this link is formalized by expressing a maximum response as the product of an RMS scale and a dimensionless peak factor that depends on bandwidth, duration, and dependence structure. Earthquake ground motion, however, introduces an additional layer of complexity. Even when one focuses on a single oscillator period and damping level, the horizontal excitation is inherently two-dimensional, and the response amplitude depends on the orientation of the analysis axis. As a result, the "peak" response is both a temporal extreme and a directional field.

This directional dependence is not a niche detail. It directly affects how recorded motions are summarized, how ground-motion models (GMMs) are calibrated, how probabilistic seismic hazard analysis (PSHA) aggregates epistemic and aleatory uncertainty, and how design spectra are interpreted and applied. Most modern applications require a scalar intensity measure (IM) that represents the two horizontal components, but there is no single universally "correct" scalar definition. A large literature has therefore developed around horizontal-component definitions and "orientation-independent" measures.

The practical importance of these definitions is reflected in extensive work on conversion relationships between alternative horizontal-component intensity measures (Ims). Beyer and Bommer (2006)

[1] Earthquake Engineering Research Center, Faculty of Civil and Environmental Engineering, University of Iceland, Austruvegur 2a, 800 Selfoss, Iceland, rajesh@hi.is

synthesized relationships among many component definitions and emphasized consistency requirements when combining GMMs in logic trees or preparing input for biaxial structural analysis. Watson-Lamprey and Boore (2007) provided conversion factors between orientation-independent geometric-mean measures and quantities intended to represent randomly oriented components or maximum possible single-direction response. Boore (2010)introduced nongeometric-mean rotation-independent measures (RotDnn and RotInn), including RotD50 and RotD100, which span the full range of rotated spectral amplitudes and align more directly with "maximum-direction" concepts used in practice. Later work expanded and refined these relationships using the NGA-West2 database and highlighted modest but systematic period-, magnitude-, and distance-dependence in key ratios such as RotD100/RotD50(Boore & Kishida, 2017; Shahi & Baker, 2014). In parallel, code-oriented discussions have addressed how best to represent bidirectional excitation for design spectra, including whether maximum-direction measures should be used and how they relate to the scalar measures used in GMM calibration(Stewart et al., 2011). Near-fault studies further show that directionality and maximum-direction demand can be particularly consequential in the vicinity of strong directivity effects (Huang et al., 2008).

More recent work has emphasized that directionality is not only a descriptive feature of rotated spectra, but can be incorporated directly into hazard- and design-relevant workflows. Poulos and Miranda (2021)revisited practical relationships among rotated and commonly used horizontal-component measures through the lens of two-axis structural demand and introduced MaxRotD50-type concept to better reflect the probability that at least one principal structural axis experiences an unfavorable orientation. Poulos and Miranda (2022) proposed and evaluated an orientation-independent intensity measure specifically motivated by earthquake-resistant design considerations, and further provided a probabilistic characterization of spectral directionality suitable for model-based use. Subsequent studies demonstrated that the orientation of maximum spectral response can exhibit systematic behavior, including style-of-faulting effects and predictable alignment tendencies for certain source types (Poulos & Miranda, 2023). In a complementary direction, Rupakhety and Sigbjörnsson (2013, 2014)developed rotation-invariant formulations based on resultant oscillator response, yielding expected and maximum horizontal response spectra that are invariant to sensor orientation. Together, these studies underscore that directionality influences not just "how we summarize records," but also how we map intensities into engineering demand and risk, motivating the need for a deeper stochastic understanding of the directional processes underlying rotated peak response.

This paper addresses that gap by focusing on the directional peak-factor field as a function of oscillator period and horizontal orientation. We define the directional peak factor as the ratio of a direction-dependent peak spectral ordinate to the corresponding direction-dependent RMS scale. Working in log-space, we treat the directional fluctuation of the peak factor as a π-periodic random field over orientation, and we characterize its angular dependence using correlation functions and harmonic (Fourier) representations constrained by even-harmonic symmetry. This framework enables (i) empirical quantification of angular smoothness and correlation length; (ii) identification of dominant angular harmonics and their interpretation; and (iii) estimation of an effective number of independent directions that governs statistical efficiency when summarizing over orientation (e.g., for RotD-type IMs). These results provide a principled explanation for why rotated spectra exhibit strong dependence across angles, why only a small number of angular degrees of freedom dominate, and how directionality-related uncertainty should be interpreted when developing or applying rotation-invariant measures. By explicitly isolating and characterizing the directional peak-factor field, this study provides a missing structural link for interpreting empirical directionality ratios and rotation-invariant measures.

The remainder of the paper is organized as follows. Section 2 reviews theoretical foundations for peak factors and summarizes the state of practice for horizontal-component definitions and orientation-independent measures, with emphasis on directionality models and their implications for hazard and design. Section 3 describes the dataset and computational workflow. Sections 4–6 develop the

directional peak-factor field, characterize its angular dependence and correlation structure, and analyse its harmonic representation, effective dimensionality, and distributional properties.

2. Background and Literature Review

Peak factors arise when relating an extreme (typically a maximum over a time window) to a second-order scale such as the standard deviation of a process. For stationary Gaussian processes, the foundations of level-crossing and extreme-value approximations are classical. Rice's (1944) analyses of random noise provided key expressions for expected crossing rates and related statistics that underpin many later results for maxima and excursions. Cartwright and Longuet-Higgins (1956) studied the statistical distribution of maxima of random functions, providing a bridge between spectral characterizations and extreme-value behavior. Davenport (1964) introduced practical approximations for the distribution of the largest value of a random function in the context of wind engineering, popularizing engineering "gust/peak factor" concepts. Vanmarcke (1975) advanced first-passage and extreme-value approximations using spectral moments and bandwidth measures, supporting practical calculation of peak factors via compact descriptors such as effective bandwidth and duration.

In earthquake engineering, peak factors appear in several related contexts, notably in random vibration theory (RVT). RVT approximates response-spectrum ordinates (or other peak responses) as the product of an RMS response and a peak factor that maps second-order statistics to expected maxima over a finite duration. In classical stochastic ground-motion simulation methods (e.g., Boore, 2003), the RMS is linked to the Fourier amplitude spectrum via Parseval's theorem. The peak factor is commonly expressed in terms of the expected number of zero crossings and extrema, and therefore depends on bandwidth and effective duration. Modern RVT treatments emphasize that peak factors are not universal constants: they vary with oscillator period, the spectrum of the input, and the nonstationary character of strong motion, which is often handled via effective-duration adjustments or equivalent-stationary approximations (e.g., Boore & Thompson, 2015; Kottke et al., 2021).

Peak factors control the extremes even when RMS measures are fixed. In other words, two processes can have the same variance yet different maxima because their temporal dependence (bandwidth, correlation time, intermittency) differs. When the excitation is vector-valued and one considers response along an arbitrary horizontal direction, the process seen by an oscillator depends on the projection of the horizontal ground motion onto that direction. The RMS scale in that direction is governed by the second-order structure of the two-component motion (i.e., the covariance matrix as a function of frequency/period), but the peak factor depends on the temporal structure of the projected process and thus can vary with direction even when RMS anisotropy is small. This motivates treating the directional peak factor as a field over orientation rather than as a scalar.

A separate but related literature addresses directionality as a phenomenon: the extent to which response spectra vary with orientation, how the maximum direction is distributed, and whether maximum-direction response has preferred alignment (e.g., fault-normal) in some scenarios. This literature is motivated by both physical considerations (radiation pattern, rupture directivity, path and basin effects, and site-specific polarization) and by engineering needs (maximizing structural demand over unknown alignment and ensuring consistency between hazard IMs and design spectra). Huang et al. (2008) examined maximum spectral demand in the near-fault region and documented conditions under which maximum-direction effects are pronounced.

Within the NGA-West2 project, Shahi and Baker (2014)developed empirical models for ground-motion directionality, including period-dependent behaviour of ratios such as RotD100/RotD50 and aspects of the distribution of the orientation of maximum response. Their work supports practical conversion of median-like GMM predictions to maximum-direction demands and clarifies how directionality behaves across magnitude, distance, and other predictors. Together with synthesis studies such as Boore and Kishida(2017), these results have become part of the "working toolkit" used when

practitioners need to translate between the IM used by a GMM and the IM required by a particular design or assessment procedure.

While these directionality models are highly useful, they are primarily framed in terms of amplitude ratios and empirical regression fits. They do not directly resolve how much of the orientation variability arises from second-order (RMS) anisotropy versus the stochastic structure of temporal extremes. This distinction matters as RMS anisotropy can often be interpreted geometrically (e.g., through the eigen structure of a covariance matrix over a period band), whereas peak-factor variability reflects how the extreme-value behaviour of a projected process changes with orientation. In particular, even when RMS anisotropy is modest, a direction-dependent peak factor can still modify the distribution of RotD-type quantities and influence the uncertainty of maxima or quantiles over orientation.

This study complements existing directionality and rotation-invariant formulations by providing an explicit separation between sustained (RMS) and opportunistic (peak) mechanisms. By decomposing direction-dependent peak response into an RMS scale and a direction-dependent peak factor, the analysis separates (a) persistent or slowly varying anisotropy associated with second-order geometry from (b) stochastic anisotropy associated with extreme-value behaviour.

3. Data

The dataset consists of 2182 pairs of horizontal strong-motion records from 229 earthquakes drawn from the Engineering Strong-Motion (ESM, Luzi et al., 2016) database, a pan-European repository providing uniformly processed and quality-controlled accelerometric records, selected using moment magnitude $M_w > 5.2$ and Joyner–Boore distance $R_{JB} < 110$ km criteria. For each record, 5% damped linear elastic response spectra were computed over a dense grid of oscillator periods (100 periods log-spaced between 0.01s and 10s) and orientation angles (1° increment). Magnitude and distance distribution of the dataset is shown in Figure 1.

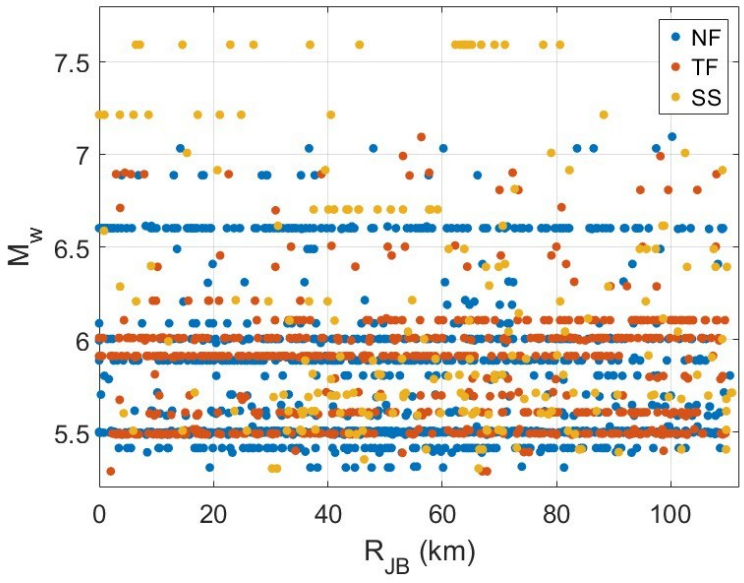

Figure 1 Scatter of event moment magnitude M_w versus Joyner–Boore distance R_{JB} for the dataset used in the study. Points are color-coded by focal mechanism: NF (normal), TF (reverse/thrust), and SS (strike-slip).

4. Directional Peak-Factor Field

Existing studies of ground-motion directionality are typically formulated directly in terms of directional spectral amplitudes or ratios of rotated spectra. While this perspective is natural from an applications standpoint, it implicitly combines two distinct sources of directional variability: (i) variation of second-order response measures with orientation, associated with the geometry of the two horizontal components, and (ii) variation in the stochastic amplification that maps those second-order measures to extreme response levels. To disentangle these effects, we focus on the directional peak factor.

For a given oscillator period T and orientation angle θ, let $S(T,\theta)$ denote the 5% damped response spectral ordinate and $\sigma(T,\theta)$ the corresponding root-mean-square (over time) response measure. The directional peak factor $p(T,\theta)$ is defined as

$$p(T,\theta) := \frac{S(T,\theta)}{\sigma(T,\theta)} \tag{1}$$

In Equation 1, $S(T,\theta)$ can be replaced by any spectral ordinate (displacement, pseudo-velocity, or pseudo-acceleration). Numerical illustrations in the rest of this work are based on pseudo-acceleration. To isolate directional variability, the peak-factor field is analyzed in logarithmic space and decomposed into period-dependent component and a directional fluctuation field $\varepsilon(T,\theta)$

$$\ln p(T,\theta) = \mu_{\ln p}(T) + \varepsilon(T,\theta) \tag{2}$$

where $\mu_{\ln p}(T)$ denotes the angularly averaged component. Owing to the symmetry of horizontal ground motion, $p(T,\theta)$ and hence $\varepsilon(T,\theta)$ is π-periodic in .

4.1. Angular Dependence and Correlation Structure

Angular dependence of the fluctuation field $\varepsilon(T,\theta)$ is quantified using angular autocorrelation as a function of angular separation. A natural second-moment definition of angular autocorrelation is

$$C_{\varepsilon}(T,\Delta\theta) = \frac{\mathbb{E}_{\theta}\left[\varepsilon(T,\theta)\ \varepsilon(T,\theta+\Delta\theta)\right]}{\mathrm{Var}_{\theta}\left[\varepsilon(T,\theta)\right]} \tag{3}$$

where $\mathbb{E}_{\theta}[.]$ and $\mathrm{Var}_{\theta}[.]$ represent expectation and variance with respect to orientation. While Eq. (3) provides a natural population-level definition, direct empirical evaluation using sample means and variances is sensitive to localized directional extremes and record-to-record scale variability. To obtain a stable estimate of the underlying angular dependence structure, we therefore introduce a robust, median-based estimator. For each record *r* and period *T*, the directional fluctuation field is first centered using the angular median,

$$\varepsilon_r(T,\theta) = \ln p_r(T,\theta) - \underset{\theta}{\mathrm{med}}\left[\ln p_r(T,\theta)\right] \tag{4}$$

such that $\underset{\theta}{\mathrm{med}}\left[\varepsilon_r(T,\theta)\right]$ is 0 by construction. A robust scale surrogate is then defined using the median absolute deviation (MAD)

$$\mathrm{MAD}_{\varepsilon_r}(T) = \underset{\theta}{\mathrm{med}}\left(\left|\varepsilon_r(T,\theta)\right|\right). \tag{5}$$

The normalized fluctuation field is given by

$$E_r(T,\theta) := \frac{\varepsilon_r(T,\theta)}{\mathrm{MAD}_{\varepsilon_r}(T)}. \tag{6}$$

A robust angular correlation estimate for each record is obtained as

$$C_r(T,\Delta\theta) := \underset{\theta}{\mathrm{med}}\left[E_r(T,\theta)\,E_r(T,\theta+\Delta\theta)\right] \tag{7}$$

and the final angular autocorrelation function is defined as the median across records,

$$\tilde{C}_\varepsilon := \underset{r}{\mathrm{med}}\left[C_r(T,\Delta\theta)\right] \tag{8}$$

Figure 2 illustrates the angular dependence of the directional fluctuation field through the median-based angular autocorrelation function defined in Eq. (8). The correlation is shown as a function of angular separation $\Delta\theta$ for several representative oscillator periods.

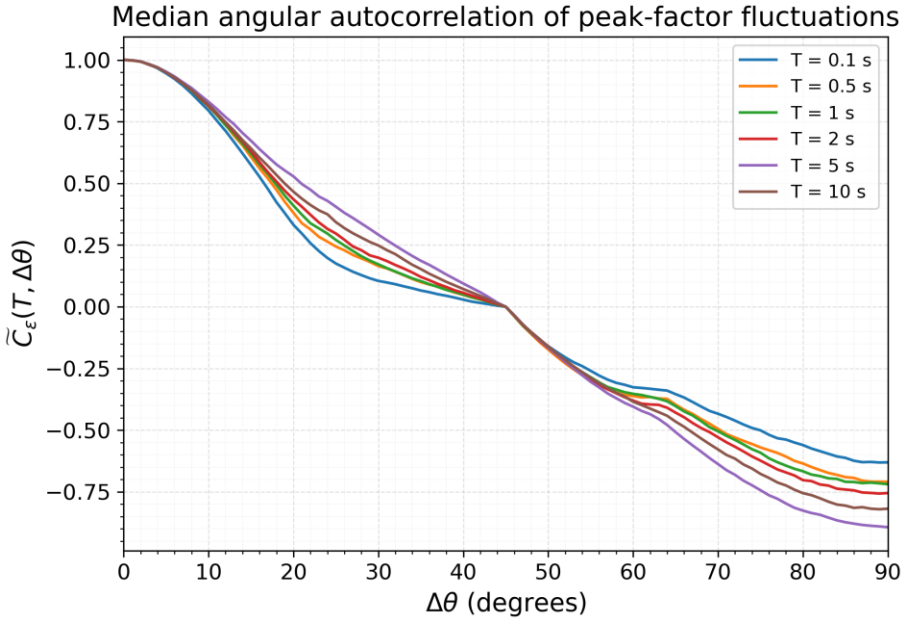

Figure 2 Median angular autocorrelation $\tilde{C}_\varepsilon(T,\Delta\theta)$ of the directional fluctuation field $\varepsilon(T,\theta)$, plotted as a function of angular separation $\Delta\theta$ for selected oscillator periods T.

The angular autocorrelation exhibits a smooth decay with increasing angular separation, transitioning from strong positive correlation at small $\Delta\theta$ to negative correlation at larger separations. A systematic zero crossing occurs at 45°, followed by a pronounced negative lobe approaching $\Delta\theta = 90^\circ$. The similarity of the correlation shape across periods suggests a consistent low-dimensional angular dependence, with modest period-to-period differences reflecting variations in the strength of directional coherence.

4.2. Harmonic Structure and Effective Number of Directions

Angular autocorrelation functions provide a compact diagnostic of directional dependence, but they do not directly identify the angular modes responsible for the structure identified in Section 4.1. A complementary and more revealing perspective is obtained by decomposing the directional fluctuation field into angular harmonics. This representation identifies the dominant angular modes governing directional peak-factor variability and their effective dimensionality.

Because horizontal ground-motion response is invariant under a rotation of 180°, the directional peak-factor field is π-periodic by construction. This symmetry constrains the admissible angular structure of the fluctuation field and implies that only even angular harmonics can contribute to its Fourier representation. As a result, the lowest-order nontrivial angular mode corresponds to a 2θ dependence.

For each record $r$and period T, the normalized fluctuation field can be expressed as a Fourier sum

$$E_r\left(T,\theta\right)=\sum_{n=1}^{\infty}\left[a_{2n,r}\left(T\right)\cos\left(2n\theta\right)+b_{2n,r}\left(T\right)\sin\left(2n\theta\right)\right] \tag{9}$$

where $a_{2n,r}\left(T\right)$ and $b_{2n,r}\left(T\right)$ are record-dependent harmonic coefficients. Each harmonic term in Eq. (9) corresponds to a distinct angular pattern of directional variability. The 2θ harmonic represents the simplest nontrivial angular dependence, characterized by two lobes of opposite sign over a π-period. Higher-order harmonics introduce progressively finer structure.

The harmonic representation in Eq. (9) enables direct quantification of the relative importance of different angular modes in governing directional peak-factor variability. For each record $r$and period T, the contribution of the $2n\theta$ harmonic is quantified through its harmonic energy,

$$\mathbf{E}_{2n,r}\left(T\right)=a_{2n,r}^2\left(T\right)+b_{2n,r}^2\left(T\right) \tag{10}$$

To remove record-specific amplitude effects and facilitate comparison across periods, harmonic energies are normalized by the total angular energy for each record, yielding per-record harmonic energy fractions

$$w_{2n,r}\left(T\right)=\frac{\mathbf{E}_{2n,r}\left(T\right)}{\sum_{m=1}^{\infty}\mathbf{E}_{2m,r}\left(T\right)} \tag{11}$$

The typical contribution of each angular harmonic is then summarized across the dataset using the median over records

$$W_{2n}=\underset{r}{\mathrm{med}}\left[w_{2n,r}\left(T\right)\right] \tag{12}$$

The quantity $W_{2n}(T)$represents the fraction of directional peak-factor variability carried by the $2n\theta$ harmonic for a typical ground-motion record. Dominance of the lowest-order harmonic corresponds to $W_2(T)$ approaching unity, while rapidly decaying contributions from higher-order harmonics indicate a low-dimensional angular structure.

Figure 3 illustrates the resulting harmonic energy fractions $W_{2n}(T)$ for a range of representative oscillator periods. The left panel shows the decay of median harmonic contributions with increasing harmonic order for selected periods, while the right panel summarizes the same information as a function of period and harmonic order.

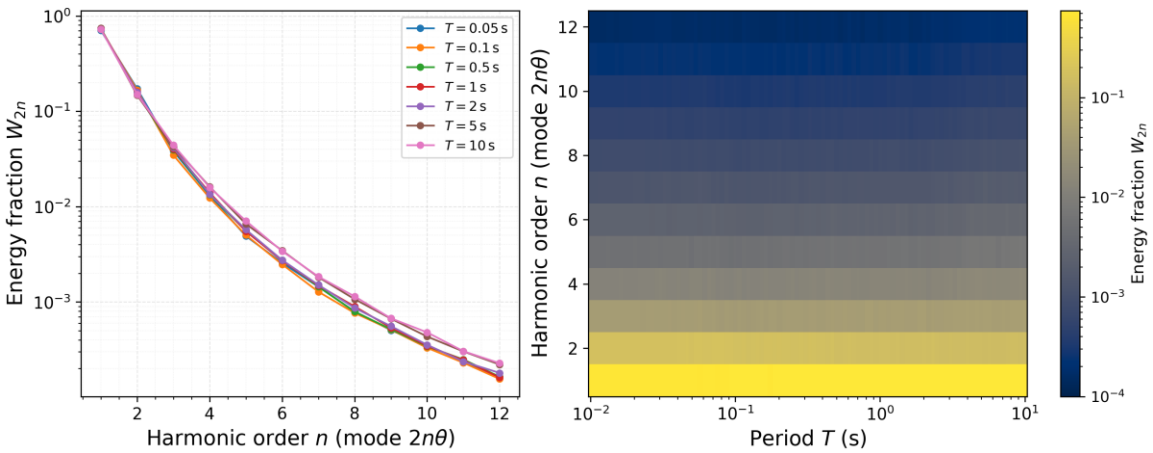

Figure 3 Median harmonic energy fractions $W_{2n}(T)$of the robustly normalized directional fluctuation field $E_r(T,\theta)$.

Figure 3 shows that directional peak-factor variability is dominated by the lowest-order angular harmonic across the full range of oscillator periods considered. For all periods, the 2θmode accounts for most of the angular energy, with harmonic contributions decaying rapidly as harmonic order increases. Higher-order modes contribute only marginally, with energy fractions decreasing by several orders of magnitude over the first few harmonics. The dominance of the lowest admissible angular harmonic is consistent with the single zero crossing observed in the angular autocorrelation functions, as discussed in Section 4.1.

4.3 Effective number of directions

Although directional spectra are often evaluated over many uniformly spaced orientations, the results presented above demonstrate that these directions are highly correlated. As a result, the nominal number of sampled directions substantially overestimates the amount of independent directional information contained in a ground-motion record. A more meaningful characterization is obtained by quantifying the effective number of directions, defined as the number of independent angular degrees of freedom implied by the observed angular structure of the fluctuation field.

Several measures of effective dimensionality are commonly used to summarize distributions over modes, including entropy-based measures, participation ratios, and cumulative energy thresholds. In the present context, the effective number of directions should provide a simple, interpretable scalar measure that reflects how directional variability is distributed across angular harmonics.

To quantify the dimensionality of directional peak-factor variability implied by the harmonic energy distribution, we define an effective number of directions based on the inverse participation ratio of the harmonic energy fractions. Specifically, for a record r, the effective number of directions at period T is defined as

$$N_{ef,r}(T) = \left(\sum_n w_{2n,r}^2(T) \right)^{-1} \tag{13}$$

and a representative value across the records is defined as

$$N_{eff}(T) = \underset{r}{\text{med}} \left[N_{eff,r}(T) \right] \tag{14}$$

This measure equals unity when directional variability is entirely concentrated in a single angular mode and increases as energy is distributed across a larger number of harmonics. The effective number of directions defined above does not represent a physical count of discrete orientations, but rather a measure of angular dimensionality implied by the observed directional dependence.

Figure 4 shows the effective number of directions implied by the angular structure of directional peak-factor fluctuations, together with record-to-record variability. The median effective number of directions remains close to two across the full range of oscillator periods, indicating that directional peak-factor variability is intrinsically low-dimensional. The relatively narrow interquartile range shows that this behaviour is consistent across records, while the broader 10–90% range reflects natural variability in angular structure among individual ground motions.

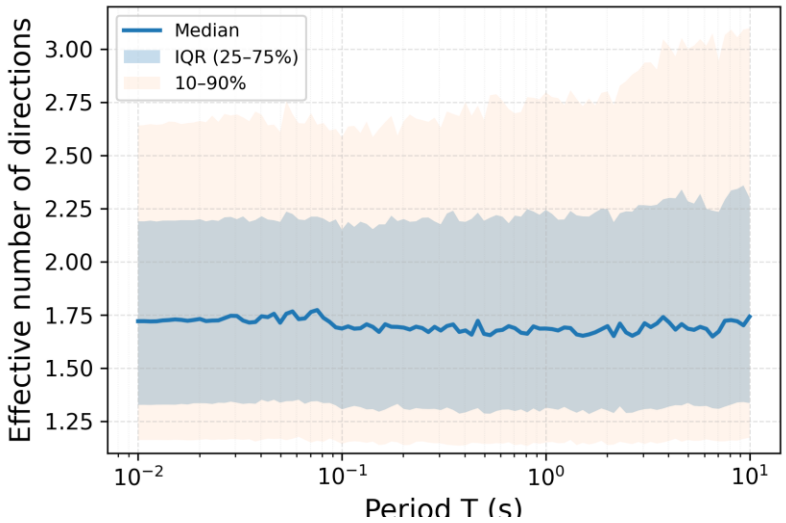

Figure 4. Effective number of directions $N_{\mathrm{eff}}(T)$implied by the angular structure of directional peak-factor fluctuations, shown as a function of oscillator period.

5 Structure of the dominant angular harmonic

Motivated by the strong dominance of the first admissible angular harmonic established in the previous section, we approximate the fluctuation field $\varepsilon\left(T,\theta\right)$ by its leading component. This yields a compact parameterization of the dominant directional anisotropy in terms of an amplitude and an orientation (phase). For each record *r* and period *T*, we adopt the leading-harmonic approximation

$$\varepsilon_r\left(T,\theta\right)\approx a_{2,r}\left(T\right)\cos 2\theta+b_{2,r}\left(T\right)\sin 2\theta \tag{15}$$

with an associated dominant anisotropy amplitude

$$\rho_r\left(T\right)=\sqrt{a_{2,r}^2\left(T\right)+b_{2,r}^2\left(T\right)} \tag{16}$$

and its orientation (phase)

$$\phi_r\left(T\right)=\frac{1}{2}\operatorname{atan2}\left(b_{2,r}\left(T\right),a_{2,r}\left(T\right)\right),\quad \phi_r\left(T\right)\in[0,\frac{\pi}{2}) \tag{17}$$

To further assess the physical significance of the dominant angular harmonic, we examine the structure of the directional fluctuation field after explicit alignment by its record-specific preferred orientation. For each ground-motion record and oscillator period, the orientation of the leading harmonic is estimated from the raw fluctuation field and used to define an aligned angular coordinate. This procedure removes record-to-record variability in phase while preserving the intrinsic angular structure of the fluctuations. The aligned fields are then aggregated across records using the median, allowing the typical directional dependence to be examined directly and compared with its leading-order harmonic approximation. The results are presented in Figure 5.

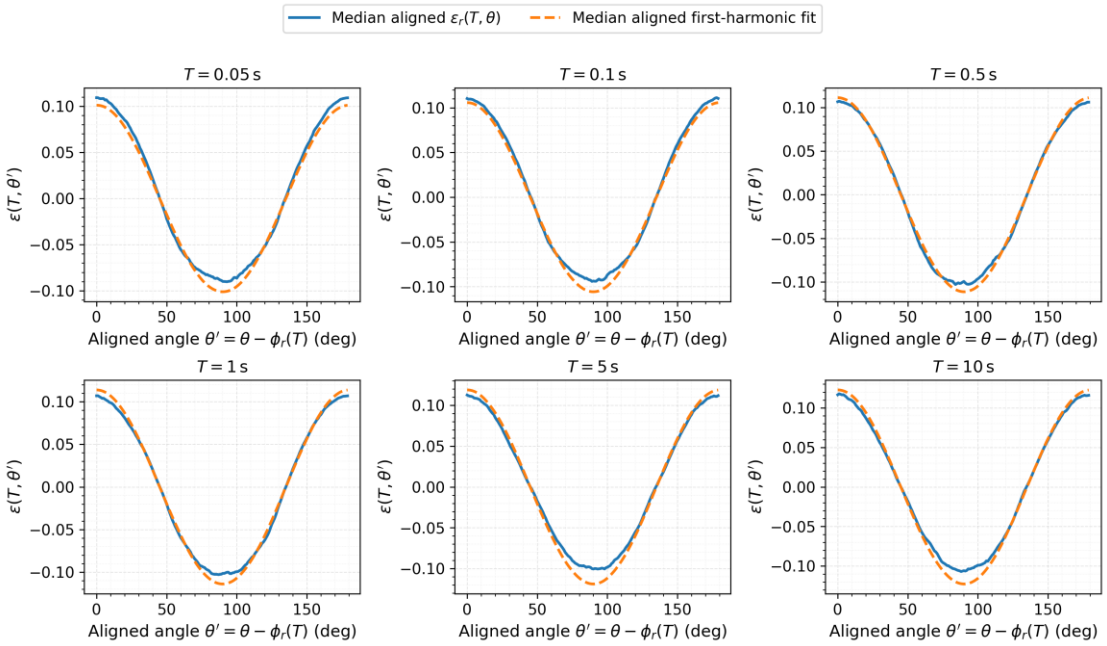

Figure 5. Median aligned directional fluctuation field compared with the corresponding median first-harmonic approximation for selected oscillator periods.

Figure 5 shows that, after alignment by the dominant harmonic orientation, the median directional fluctuation field exhibits a smooth and nearly sinusoidal dependence on the aligned angle for all periods considered. The empirical median curves are closely matched by their first-harmonic reconstructions, with excellent agreement in both amplitude and angular shape. Small and systematic deviations between the empirical median field and the first-harmonic fit indicate the presence of higher-order angular components, but their contribution is minor relative to the dominant mode. Importantly, the quality of the first-harmonic approximation is consistent across short- and long-period oscillators, indicating that the low-dimensional angular structure of directional peak-factor variability is robust and largely period-independent.

5.1 Dominant anisotropy amplitude

The amplitude $\rho_r(T)$ provides a direct measure of the strength of directional anisotropy in the directional fluctuation field. Statistical properties of the anisotropy amplitude are presented in Figure 6.

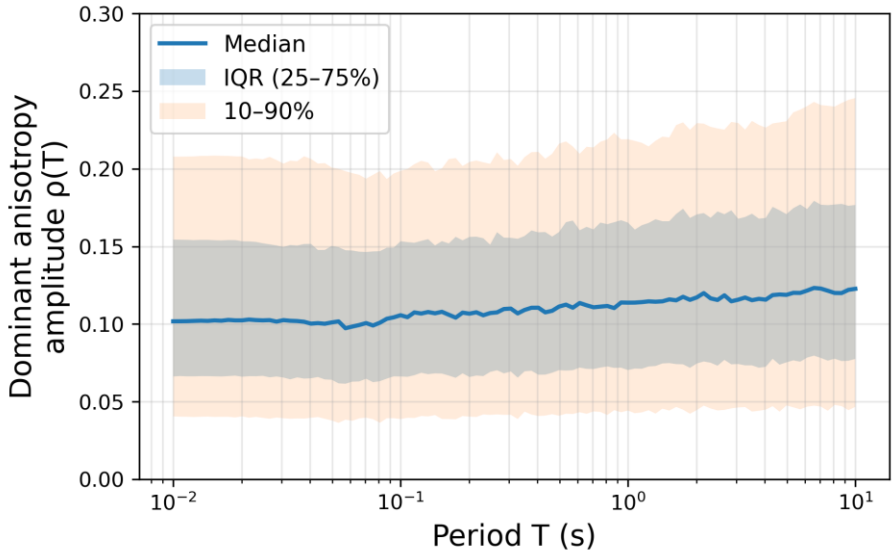

Figure 6 Distribution of the dominant anisotropy amplitude ρ(T) as a function of oscillator period. The solid line shows the median across records, while the shaded bands denote the interquartile range (25–75%) and the 10–90% range.

Figure 6 shows that the dominant anisotropy amplitude exhibits a well-defined and relatively narrow distribution across records for all oscillator periods considered. Median values of $\rho_r(T)$ remain of order 0.1 in logarithmic peak-factor space, with modest record-to-record variability as indicated by the interquartile and 10–90% ranges. The dependence of $\rho_r(T)$ on period is weak. A slight increase in the median amplitude is observed toward longer periods, but the overall variation across the spectral range is small compared to the across-record scatter.

5.2 Dominant anisotropy phase

Figure 7 illustrates the across-record distribution of the dominant anisotropy phase $\phi_r(T)$ at selected oscillator periods using violin plots.

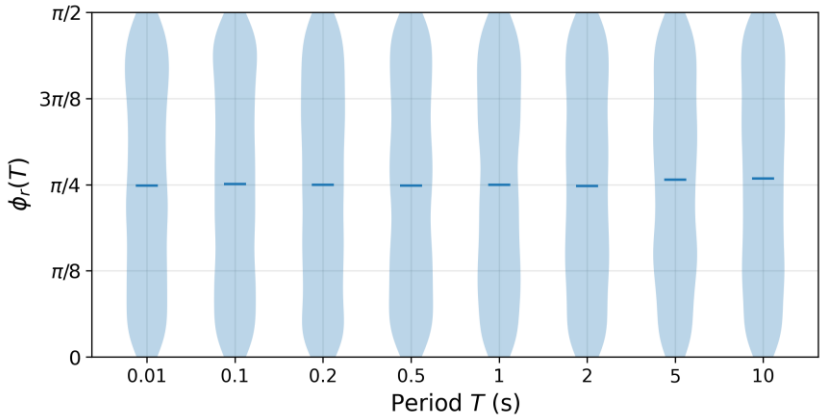

Figure 7 Violin plots of the dominant anisotropy phase $\phi_r(T)$ across records at selected oscillator periods. The horizontal bars indicate the median in each violin.

The phase distributions are broadly spread over the full admissible range $[0, \pi/2)$ at all periods considered, with no evident concentration toward particular angles. This indicates that, while directional peak-factor anisotropy is consistently present within individual records (as shown by the

nonzero amplitudes $\rho_r(T)$), the orientation of that anisotropy is not systematically aligned across the dataset. Instead, the dominant harmonic direction appears record-specific and effectively random at the ensemble level.

To provide a quantitative assessment of phase uniformity, we introduce a nonparametric diagnostic that measures the maximum deviation of the empirical phase distribution from the uniform distribution. For each oscillator period T, the dominant anisotropy phase $\phi_r(T)$is first rescaled to the unit interval as

$$u_r(T) = \frac{\phi_r(T)}{\pi/2}, \quad u_r(T) \in [0,1].$$

Let $F_T(u)$ denote the empirical cumulative distribution of $u_r(T)$ across records. We define a Kolmogorov-Smirnov-type deviation statistic as

$$D(T) := \sup_{u\in[0,1]} \left| F_T(u) - u \right|.$$

The quantity $D(T)$ measures the maximum absolute departure of the empirical phase distribution from the uniform distribution on [0,1]. Under the assumption of independent samples drawn from a uniform distribution, the expected magnitude of $D(T)$is controlled by the distribution-free Dvoretzky–Kiefer–Wolfowitz inequality, which provides a conservative reference threshold for deviations arising purely from finite sample size. Figure 8 shows $D(T)$ as function of oscillator period.

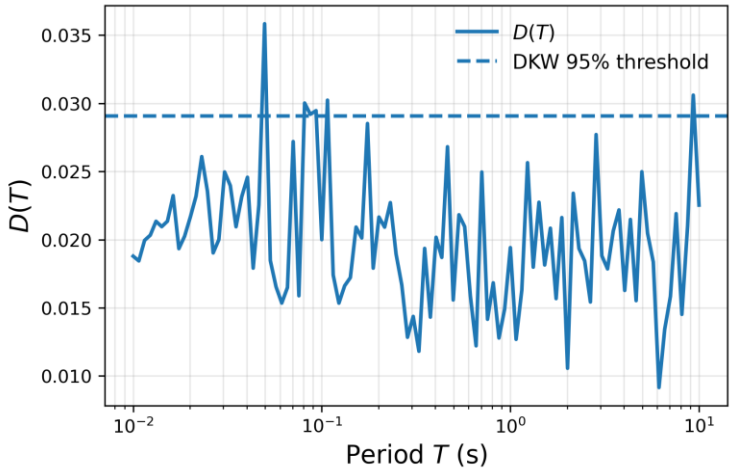

Figure 8 Period-dependent Kolmogorov–Smirnov–type deviation $D(T)$between the empirical distribution of $\phi_r(T)$and the uniform distribution on $[0, \pi/2)$. The dashed line indicates the distribution-free 95% Dvoretzky–Kiefer–Wolfowitz (DKW) threshold expected under uniformity.

In Figure 8, the deviation measure $D(T)$remains small across the full range of oscillator periods and lies predominantly below the 95% DKW threshold expected for samples drawn from a uniform distribution. Isolated excursions approaching the threshold occur sporadically and do not exhibit any systematic dependence on period. This behavior indicates that observed departures from uniformity are consistent with finite-sample variability rather than reflecting genuine directional alignment. Together with the violin plots in Figure 7, these results provide quantitative support for the conclusion that the dominant anisotropy phase $\phi_r(T)$is effectively uniform across records.

6. Distributional properties in harmonic space

We analyze the empirical distributions of $a_{2,r}(T)$ and $b_{2,r}(T)$ across records at selected periods. Because these coefficients are defined as signed projections of $\varepsilon_r(T,\theta)$onto orthogonal angular basis functions, symmetry about zero and similarity of scale between $a_{2,r}(T)$and $b_{2,r}(T)$are expected if the dominant harmonic behaves in a statistically regular manner. Deviations from symmetry or marked differences between the two coefficients would indicate departures from simple stochastic structure. Figure 9 summarizes the across-record distributions of $a_{2,r}(T)$ and $b_{2,r}(T)$ using violin plots at representative periods.

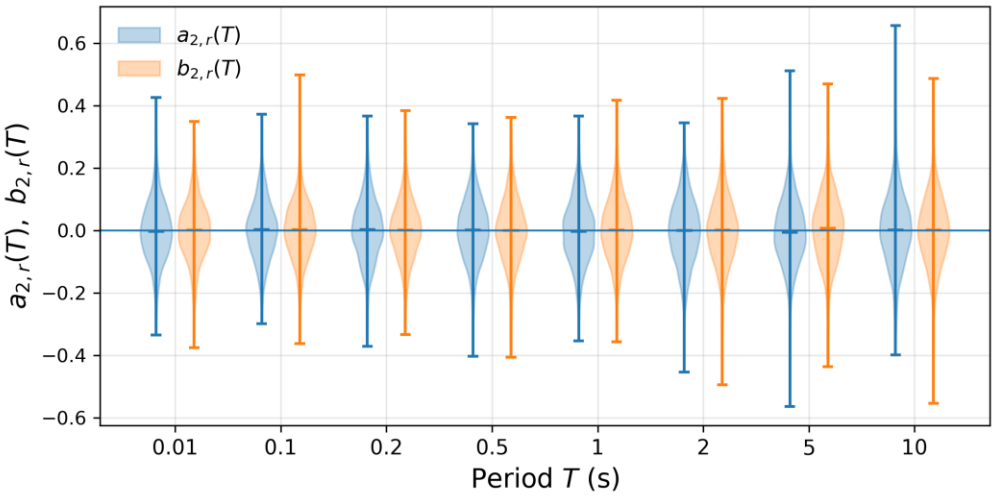

Figure 9 Across-record distributions of the first-harmonic coefficients $a_{2,r}(T)$and $b_{2,r}(T)$at selected oscillator periods, shown as side-by-side violin plots.

The coefficient distributions are approximately symmetric about zero at all periods considered, with no evident skewness or systematic offset in either $a_{2,r}(T)$or $b_{2,r}(T)$. The spreads of the cosine and sine coefficients are also broadly comparable at each period, indicating that the two quadrature components of the dominant angular harmonic contribute similarly to directional peak-factor variability across records.

Figure 10 examines the joint distribution of the first-harmonic coefficients $a_{2,r}(T)$ and $b_{2,r}(T)$ across records at representative oscillator

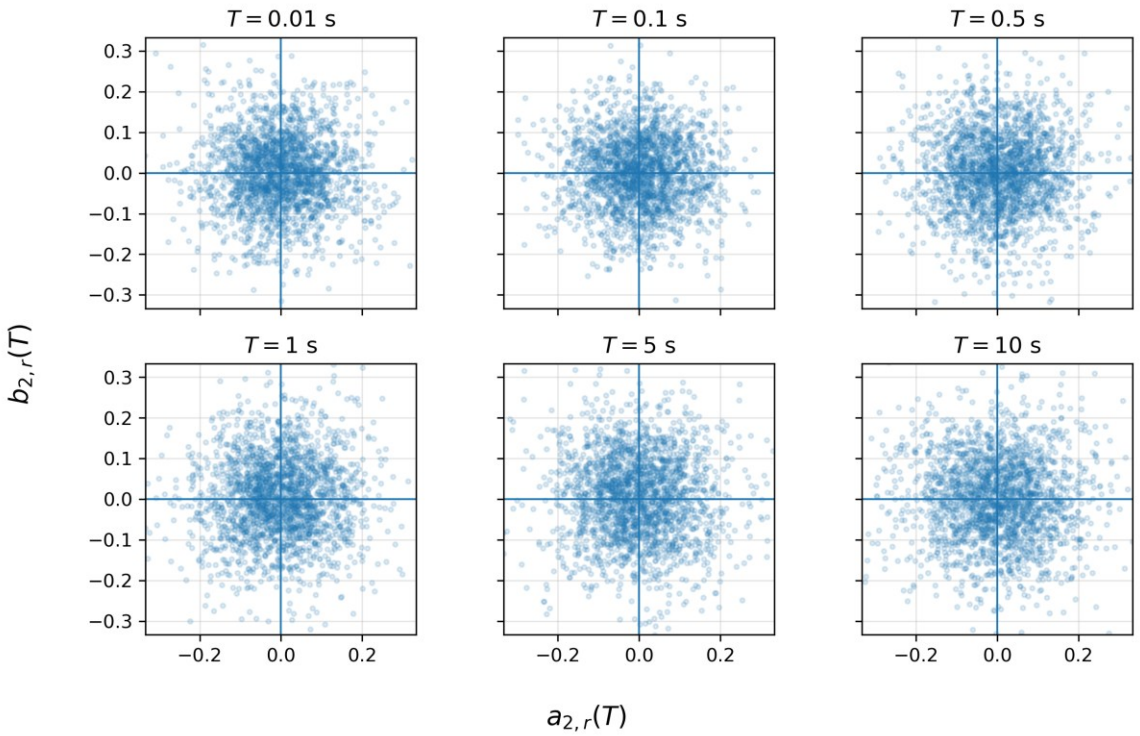

Figure 10. Joint distributions of the first-harmonic coefficients $a_{2,r}(T)$ and $b_{2,r}(T)$ across records at selected oscillator periods. Each panel shows a scatter plot of $b_{2,r}(T)$ versus $a_{2,r}(T)$ with equal axis scaling.

Across all periods shown, the joint distributions of $a_{2,r}(T)$and $b_{2,r}(T)$are centered near the origin and exhibit approximately circular symmetry, with no evident elongation or preferred orientation. This indicates the absence of systematic correlation between the cosine and sine coefficients of the dominant angular harmonic and suggests comparable variability along both coefficient directions.

These observations support a statistically isotropic description of the dominant harmonic coefficients in the cosine–sine plane, in which $\left(a_{2,r}(T), b_{2,r}(T)\right)$ behaves as a pair of approximately zero-mean random variables with similar variance and weak dependence.

Figure 11 evaluates the Gaussianity of the first-harmonic coefficients by comparing their empirical distributions to a standard normal distribution using quantile–quantile (Q–Q) plots. For each selected oscillator period, the coefficients $a_{2,r}(T)$ and $b_{2,r}(T)$ are standardized by their empirical standard deviations and plotted against the corresponding normal quantiles.

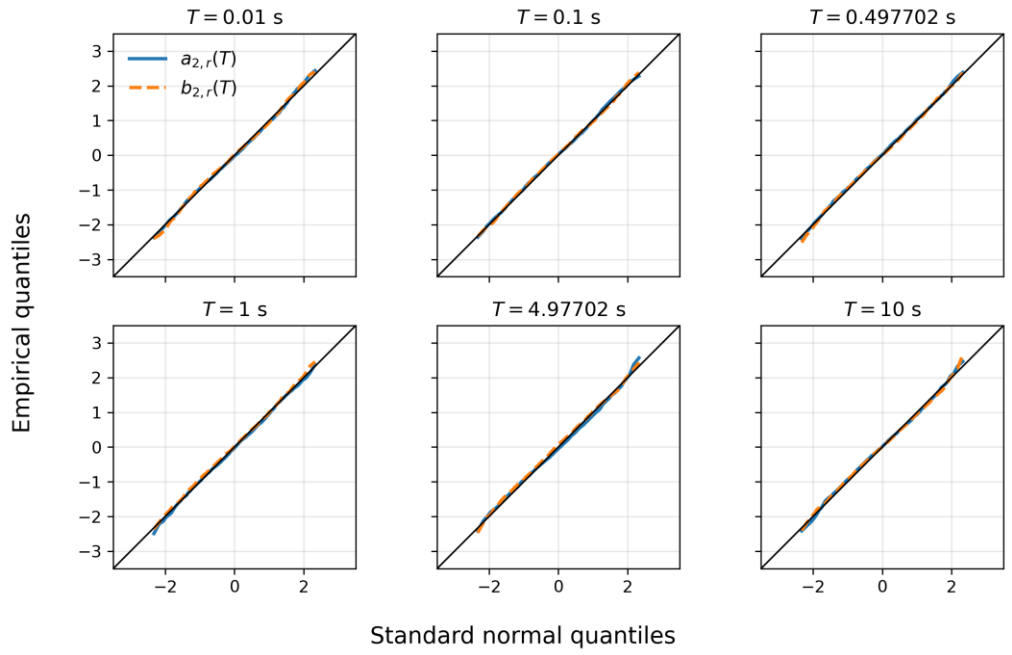

Figure 11 Normal Q–Q plots of the standardized first-harmonic coefficients $a_{2,r}(T)$ and $b_{2,r}(T)$ at selected oscillator periods. The solid line denotes the standard normal reference.

Across all periods shown, the standardized first-harmonic coefficients closely follow the standard normal distribution over the full central range, with only minor and symmetric deviations in the extreme tails. The Q–Q curves for $a_{2,r}(T)$ and $b_{2,r}(T)$ nearly coincide at each period, indicating that the cosine and sine coefficients not only share similar scale but also exhibit virtually identical distributional shape.

The results above support a compact stochastic representation of the dominant angular harmonic in which the first-harmonic coefficients behave as approximately independent, identically distributed Gaussian random variables across records

$$\begin{pmatrix} a_{2,r}(T) \\ b_{2,r}(T) \end{pmatrix} \sim N\left(\begin{pmatrix} 0 \\ 0 \end{pmatrix},\ \sigma^2(T)\mathbf{I} \right)$$

where $\sigma(T)$ is a period-dependent scale parameter and $\mathbf{I}$ denotes the identity matrix. Under this model, the dominant anisotropy amplitude $\rho_r(T)$ follows a Rayleigh distribution with scale parameter $\sigma(T)$ (Beckmann, 1964). Two complementary estimators of $\sigma(T)$ can be defined directly from the first-harmonic coefficients. First, exploiting the Rayleigh distribution of $\rho_r(T)$, a robust estimator based on the median amplitude is given by

$$\hat{\sigma}^{(\rho)}(T) = \frac{\rho_r(T)}{\sqrt{2\ln 2}}.$$

Alternatively, a moment-based estimator can be obtained directly from the coefficient pair as

$$\sigma^{(ab)}(T)=\sqrt{\frac{a_{2,r}^2(T)+b_{2,r}^2(T)}{2}}$$

which corresponds to the root-mean-square scale of the isotropic Gaussian model. Figure 12 summarizes the period dependence of the Gaussian scale parameter $\sigma(T)$ of the dominant angular harmonic using the amplitude-based estimator $\hat{\sigma}_r^{(\rho)}(T)$. The figure shows the median value across records together with the 16–84 percentile range.

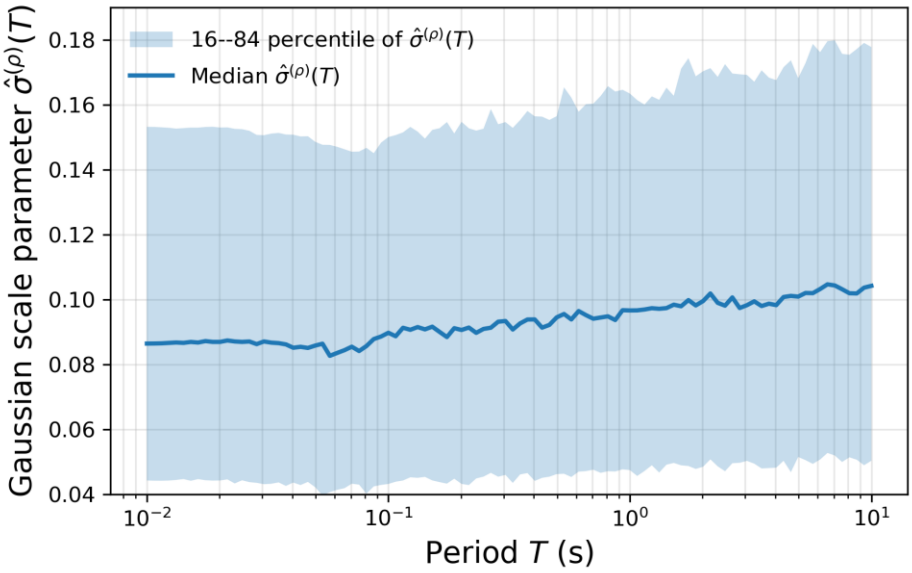

Figure 12 Period dependence of the Gaussian scale parameter $\sigma(T)$ estimated from the dominant harmonic amplitude $\rho_r(T)$. The solid line denotes the median of $\hat{\sigma}_r^{(\rho)}(T)$ across records, and the shaded band indicates the 16–84 percentile range.

The Gaussian scale parameter $\sigma(T)$ exhibits a smooth and gradual dependence on oscillator period, with median values increasing modestly from short to long periods. Across the full period range considered, the record-to-record variability remains moderate, as indicated by the relatively stable width of the 16–84 percentile band. The absence of sharp transitions or irregular features in $\sigma(T)$ suggests that the strength of stochastic directional anisotropy associated with the dominant angular harmonic varies smoothly with period.

Figure 13 assesses the robustness of the estimated Gaussian scale parameter $\sigma(T)$ under random subsampling of records. The dataset is randomly partitioned into five disjoint folds, and the median amplitude-based estimator $\hat{\sigma}^{(\rho)}(T)$ is recomputed within each fold. The resulting fold-to-fold variability is compared to the full-sample estimate as a function of period. The full-sample estimate of $\sigma(T)$ lies well within the envelope defined by the five subsampled medians across the entire period range. Although minor fold-to-fold fluctuations are observed, particularly at longer periods where sampling variability is naturally larger, the overall period dependence and magnitude of $\sigma(T)$ remain stable under random partitioning of the data.

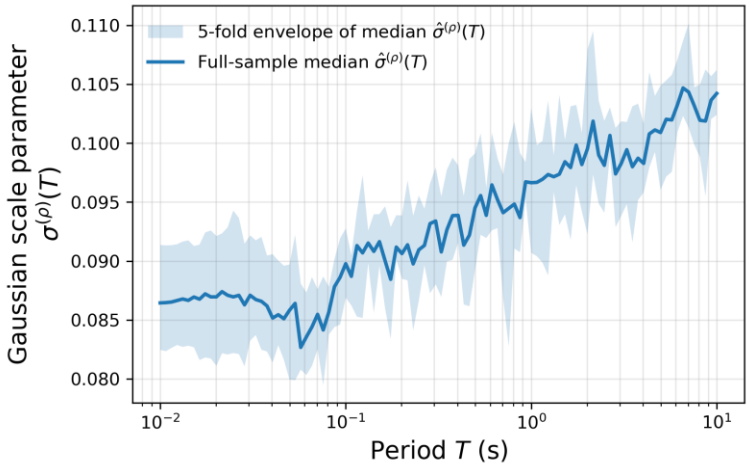

Figure 13 Stability of the Gaussian scale parameter $\sigma(T)$ under random five-fold subsampling. The solid line denotes the full-sample median of $\hat{\sigma}^{(\rho)}(T)$, and the shaded band indicates the envelope of fold-specific medians across five random partitions of the dataset.

The π -periodicity of $\varepsilon(\theta)$allows a natural decomposition with respect to a rotation by $\pi/2$. We define the symmetric and anti-symmetric components of $\varepsilon(\theta)$ as

$$\varepsilon^s\left(T,\theta\right)=\frac{\varepsilon\left(T,\theta\right)+\varepsilon\left(T,\theta+\pi/2\right)}{2},\quad \varepsilon^a\left(T,\theta\right)=\frac{\varepsilon\left(T,\theta\right)-\varepsilon\left(T,\theta+\pi/2\right)}{2} \tag{18}$$

These satisfy the identities

$$\varepsilon\left(T,\theta\right)=\varepsilon^s\left(T,\theta\right)+\varepsilon^a\left(T,\theta\right),\quad \varepsilon\left(T,\theta+\pi/2\right)=\varepsilon^s\left(T,\theta\right)-\varepsilon^a\left(T,\theta\right) \tag{19}$$

The symmetric component $\varepsilon^s\left(T,\theta\right)$ captures fluctuations that are preserved under a $\pi/2$ rotation, while the anti-symmetric component $\varepsilon^a\left(T,\theta\right)$ captures fluctuations that change sign under such a rotation. Under the dominant first-harmonic approximation for $\varepsilon(\theta)$, the anti-symmetric component can be written as

$$\varepsilon_r^a\left(T,\theta\right)=a_{2,r}\left(T\right)\cos 2\theta+b_{2,r}\left(T\right)\sin 2\theta. \tag{20}$$

Thus, the anti-symmetric component preserves exactly the same harmonic structure and stochastic coefficients as the leading approximation to the full field. In particular, $\varepsilon^a\left(T,\theta\right)$ is itself a single-harmonic random field with Gaussian coefficients, Rayleigh-distributed amplitude, and uniform phase. This observation highlights that, within the dominant-harmonic regime, the full directional fluctuation field can be reconstructed from its symmetric and anti-symmetric components without introducing additional stochastic degrees of freedom.

8. Practical implications for ground motion modelling and engineering workflows

Directional variability is often handled operationally by rotating the two horizontal components through a dense set of orientations, computing response spectra at each angle, and then applying nonlinear summaries such as medians or maxima (e.g., RotD-type measures) or repeating structural analyses for many rotated inputs. While straightforward, this workflow can unintentionally conflate angular resolution with statistical information: increasing the number of evaluated angles does not necessarily increase the amount of independent directional information extracted from a record.

8.1. Rotating ground motions through many angles does not produce many independent realizations

A frequent motivation for dense rotation is to "capture directional variability" by treating the collection of rotated spectra (or rotated structural responses) as an ensemble. The present results show that this intuition is statistically unjustified: nearby orientations are strongly dependent, and the effective dimensionality of the directional field is low. As a result, rotating a record through tens or hundreds of angles does not create tens or hundreds of independent directional outcomes; it mainly produces redundant evaluations of the same underlying low-dimensional structure. This point has two practical implications:

1. Uncertainty is not reduced by angular oversampling. If directionality is treated as an aleatory effect associated with unknown alignment, increasing the number of evaluated angles does not reduce uncertainty about directionality for that record, because the angles are not independent. In this sense, dense rotation is not a substitute for probabilistic treatment of directional uncertainty.

2. Angular "sample size" must be interpreted using effective dimensionality, not the number of angles. Any procedure that uses rotated orientations as if they were independent (e.g., in assessing sampling variability of RotD-type summaries, or in estimating within-record directional variability) should account for the strong dependence implied by the angular correlation structure and the observed low-dimensional harmonic content.

8.2 Implications for nonlinear time-history analysis (NTHA) and computational burden

In many projects, practitioners rotate ground motions repeatedly and rerun nonlinear time-history analyses to explore sensitivity to incident direction. This can quickly become a major computational and logistical burden, especially when multiple records, multiple intensity levels, and multiple structural models are involved. Given the low effective dimensionality of directional variability demonstrated above, there are diminishing returns from dense angular rotation when the intent is to represent directionality as uncertainty rather than to compute an exact worst-case over angle In practical terms:

1. If the purpose of rotation is uncertainty representation over unknown alignment, then performing dozens of rotations of the same record is an inefficient way to explore the directional space, because most rotations are strongly dependent.

2. If the purpose of rotation is worst-case search, then the smoothness of the directional field implies that maxima over angle are controlled by coherent angular structure rather than by fine-scale angular fluctuations. This suggests that very fine angular increments may be unnecessary for identifying near-maximal directions in many cases, although the required angular resolution depends on the user's tolerance for approximation error.

These points do not eliminate the need for rotation in NTHA when maximum-direction demand is required. Rather, they clarify that rotation over many angles should be viewed as a numerical search (with potential redundancy) rather than as a way to generate many independent realizations of directional demand.

8.3 Implications for interpretation and use of RotD-type measures

Rotation-invariant intensity measures such as RotD50 and RotD100 are routinely computed by evaluating spectra at many angles and then taking a percentile across angles. The present results provide a structural explanation for why RotD-type measures exhibit stable empirical behavior across datasets:

1. Strong angular dependence and low-dimensional harmonic structure explain why rotated spectra vary smoothly with angle and why only a small number of angular degrees of freedom dominate.

2. The effective dimensionality result clarifies that the distribution of RotD-type measures is controlled by the stochastic structure of the directional peak-factor field, not by the number of evaluated angles.

3. Full stochastic characterization of directional response spectra can be obtained by a small number of suitably selected parameters, for example, response spectra evaluated at a small number of physically meaningful orientations, such as the principal directions of oscillator RMS response

A related implication concerns the interpretation of directionality ratios (e.g., RotD100/RotD50). Such ratios are often treated as "conversion factors" between different component definitions. The present framework clarifies that these ratios are influenced not only by RMS response geometry but also by the directional variability of peak factors, and that the latter can remain non-negligible even when RMS anisotropy is modest.

8.4 Implications for GMPE development, residual modeling, and PSHA workflows

In hazard and ground-motion modeling contexts, directionality affects (i) how two-component recordings are summarized into a scalar IM used for GMPE calibration, and (ii) how additional uncertainty associated with directionality is propagated into risk- and design-relevant quantities. The low-dimensional angular structure documented here has two practical consequences:

1. Dependence across orientations must be respected. When assessing within-record directional variability (or when attempting to quantify the uncertainty of rotation-invariant summaries), treating rotated orientations as independent can lead to misleading uncertainty estimates.

2. Efficient probabilistic integration over orientation is plausible. Because the directional peak-factor field is well approximated by a small number of harmonic degrees of freedom, it is feasible—at least in principle—to represent directional effects using reduced-order stochastic descriptors rather than dense angle-by-angle evaluations. This perspective aligns naturally with probabilistic frameworks that integrate over latent variables rather than exhaustively sampling redundant orientations.

8.5 Practical value of separating RMS geometry from stochastic peak formation

A central finding of this work is that stochastic directional anisotropy in peak formation persists even when deterministic anisotropy in second-order (RMS) response measures is weak. This has direct practical implications:

1. It cautions against interpreting weak RMS anisotropy as evidence that maximum-direction effects will be negligible.
2. It clarifies why directionality-related variability in rotated spectra can remain appreciable even for records whose second-order response geometry is close to isotropic.
3. It motivates separating sustained (RMS) directional structure from opportunistic (peak-factor) directional structure when interpreting directionality ratios or when designing simplified directionality models.

8.6 Scope and limitations

The practical implications above are grounded in the directional structure of response-spectrum peak factors for linear elastic oscillators. While many engineering workflows (including NTHA rotation practices) use similar rotation logic, nonlinear structural response can introduce additional complexities beyond those captured by oscillator peak-factor fields alone. The present results should therefore be interpreted as (i) a rigorous characterization of directional structure underlying response spectra, and (ii) a strong indication that dense angular oversampling is statistically inefficient in many settings, rather than as a universal prescription for all nonlinear structural response problems.

9. Conclusions

This paper presents a systematic empirical characterization of the directional peak-factor field associated with horizontal response spectra. By treating directional peak factors as a stochastic field defined on the circle and analyzing their angular dependence using correlation and harmonic diagnostics, the study reveals a simple and robust structure underlying directional peak-factor variability in strong ground motion.

The main conclusions can be summarized as follows:

1. Directional peak-factor fluctuations exhibit smooth angular dependence, with strong correlation across nearby orientations and a consistent zero crossing of angular autocorrelation at 45°. This behavior shows that directional peak factors cannot be treated as independent across orientation.

2. The angular structure of directional peak-factor variability is dominated by the lowest admissible angular harmonic consistent with π-periodicity. Higher-order harmonics contribute only marginally across all oscillator periods considered.

3. As a consequence of this harmonic dominance, the effective number of independent directions governing peak-factor variability is close to unity and remains weakly dependent on period. Dense angular sampling therefore substantially overrepresents the amount of independent directional information present in a typical ground-motion record.

4. The dominant angular harmonic can be characterized by an amplitude and an orientation. The amplitude is consistently nonzero across periods, indicating persistent stochastic directional anisotropy in peak formation, while the orientation is effectively uniform across records, exhibiting no systematic alignment at the ensemble level.

5. The coefficients of the dominant angular harmonic are well described by an approximately isotropic Gaussian distribution, allowing the stochastic structure of directional peak-factor variability to be summarized by a single, smoothly varying scale parameter.

Together, these findings provide a rigorous statistical foundation for understanding directional effects in peak response that complements existing amplitude-based directionality models. By isolating the stochastic structure of directional peak factors from second-order response geometry, the analysis clarifies why directionality exhibits low-dimensional behavior, smooth period dependence, and stable empirical patterns across datasets.

References

Beckmann, P. (1964). Rayleigh distribution and its generalizations. *Journal of Research of the National Bureau of Standards, Section D: Radio Science*, *68D*(9), 927. https://doi.org/10.6028/jres.068D.092

Boore, D. M. (2003). Simulation of Ground Motion Using the Stochastic Method. *Pure and Applied Geophysics*, *160*(3), 635–676. https://doi.org/10.1007/PL00012553

Boore, D. M. (2010). Orientation-Independent, Nongeometric-Mean Measures of Seismic Intensity from Two Horizontal Components of Motion. *Bulletin of the Seismological Society of America*, *100*(4), 1830–1835. https://doi.org/10.1785/0120090400

Boore, D. M., & Kishida, T. (2017). Relations between Some Horizontal ‐ Component Ground ‐ Motion Intensity Measures Used in Practice. *Bulletin of the Seismological Society of America*, *107*(1), 334–343. https://doi.org/10.1785/0120160250

Boore, D. M., & Thompson, E. M. (2015). Revisions to Some Parameters Used in Stochastic ‐ Method Simulations of Ground Motion. *Bulletin of the Seismological Society of America*, *105*(2A), 1029–1041. https://doi.org/10.1785/0120140281

Cartwright, D. E., & Longuet-Higgins, M. S. (1956). The statistical distribution of the maxima of a random function. *Proceedings of the Royal Society of London. Series A. Mathematical and Physical Sciences*, *237*(1209), 212–232. https://doi.org/10.1098/rspa.1956.0173

Davenport, A. G. (1964). Note on the Distribution of the Largest Value of a Random Function. *Proceedings of the Institution of Civil Engineers*, *28*(2), 187–196. https://doi.org/10.1680/iicep.1964.10112

Huang, Y.-N., Whittaker, A. S., & Luco, N. (2008). Maximum Spectral Demands in the Near-Fault Region. *Earthquake Spectra*, *24*(1), 319–341. https://doi.org/10.1193/1.2830435

Kottke, A. R., Abrahamson, N. A., Boore, D. M., Bozorgnia, Y., Goulet, C. A., Hollenback, J., Kishida, T., Ktenidou, O. J., Rathje, E. M., Silva, W. J., Thompson, E. M., & Wang, X. (2021). Selection of Random Vibration Theory Procedures for the NGA-East Project and Ground-Motion Modeling. *Earthquake Spectra*, *37*(SI), 1420–1439. https://doi.org/10.1177/87552930211019052

Luzi, L., Puglia, R., Russo, E., D'Amico, M., Felicetta, C., Pacor, F., Lanzano, G., Çeken, U., Clinton, J., Costa, G., Duni, L., Farzanegan, E., Gueguen, P., Ionescu, C., Kalogeras, I., Özener, H., Pesaresi, D., Sleeman, R., Strollo, A., & Zare, M. (2016). The Engineering Strong‐Motion Database: A Platform to Access Pan‐European Accelerometric Data. *Seismological Research Letters*, *87*(4), 987–997. https://doi.org/10.1785/0220150278

Poulos, A., & Miranda, E. (2021). Relations between MaxRotD50 and Some Horizontal Components of Ground-Motion Intensity Used in Practice. *Bulletin of the Seismological Society of America*, *111*(4), 2167–2176. https://doi.org/10.1785/0120200364

Poulos, A., & Miranda, E. (2022). Proposal of orientation-independent measure of intensity for earthquake-resistant design. *Earthquake Spectra*, *38*(1), 235–253. https://doi.org/10.1177/87552930211038240

Poulos, A., & Miranda, E. (2023). Effect of Style of Faulting on the Orientation of Maximum Horizontal Earthquake Response Spectra. *Bulletin of the Seismological Society of America*, *113*(5), 2092–2105. https://doi.org/10.1785/0120230001

Rice, S. O. (1944). Mathematical Analysis of Random Noise. *The Bell System Technical Journal*, *23*(3), 282–332.

Rupakhety, R., & Sigbjörnsson, R. (2013). Rotation-Invariant Measures of Earthquake Response Spectra. *Bulletin of Earthquake Engineering*, *11*(6), 1885–1893. https://doi.org/10.1007/s10518-013-9472-1

Rupakhety, R., & Sigbjörnsson, R. (2014). Rotation-invariant mean duration of strong ground motion. Bulletin of Earthquake Engineering, 12(2), 573–584. https://doi.org/10.1007/s10518-013-9521-9

Shahi, S. K., & Baker, J. W. (2014). NGA-West2 Models for Ground Motion Directionality. *Earthquake Spectra*, *30*(3), 1285–1300. https://doi.org/10.1193/040913EQS097M

Stewart, J. P., Abrahamson, N. A., Atkinson, G. M., Baker, J. W., Boore, D. M., Bozorgnia, Y., Campbell, K. W., Comartin, C. D., Idriss, I. M., Lew, M., Mehrain, M., Moehle, J. P., Naeim, F., & Sabol, T. A.

(2011). Representation of Bidirectional Ground Motions for Design Spectra in Building Codes. *Earthquake Spectra*, *27*(3), 927–937. https://doi.org/10.1193/1.3608001

Vanmarcke, E. H. (1975). On the Distribution of the First-Passage Time for Normal Stationary Random Processes. *Journal of Applied Mechanics*, *42*(1), 215–220. https://doi.org/10.1115/1.3423521

Funding

Rajesh Rupakhety acknowledges support from the University of Iceland Research Fund.

Competing Interests

The authors have no relevant financial or non-financial interests to disclose.

Data Availability

All ground motion data used in this research are publicly available at the European Strong Motion database, https://esm-db.eu/#/home

Author Contribtions

Rajesh Rupakhety: Conceptualization, methodology, coding, manuscript writing and editing. Victor M Hernández-Aguirre: Data collection and processing, manuscript writing and editing.